

Electromagnetic torque ripple and copper losses reduction in permanent magnet synchronous machines

J. R. B. A. Monteiro^{*,†}, A. A. Oliveira Jr., M. L. Aguiar and E. R. Sanagiotti

Department of Electrical Engineering, School of Engineering of São Carlos (EESC), University of São Paulo (USP), São Carlos, SP 13566 90, Brazil

SUMMARY

This paper presents a method for electromagnetic torque ripple and copper losses reduction in (non-sinusoidal or trapezoidal) surface-mount permanent magnet synchronous machines (SM-PMSM). The method is based on an extension of classical dq transformation that makes it possible to write a vectorial model for this kind of machine (with a non-sinusoidal back-EMF waveform). This model is obtained by the application of that transformation in the classical machine per-phase model. That transformation can be applied to machines that have any type of back-EMF waveform, and not only trapezoidal or square-wave back-EMF waveforms. Implementation results are shown for an electrical converter, using the proposed vectorial model, feeding a non-sinusoidal synchronous machine (brushless DC motor). They show that the use of this vectorial mode is a way to achieve improvements in the performance of this kind of machine, considering the electromagnetic torque ripple and copper losses, if compared to a drive system that employs a classical six-step mode as a converter. Copyright © 2011 John Wiley & Sons, Ltd.

KEY WORDS: electrical drives; brushless DC motor; permanent magnet synchronous machine; vectorial control; copper losses; electromagnetic torque ripple

1. INTRODUCTION

Surface-mount permanent magnet synchronous machines (SM-PMSM) are widely used in special applications as high-precision positioning systems or in applications where efficiency is a primary need. SM-PMSMs present a low rotor inertia momentum, a high dynamic performance, and a high relation between power and weight [1,2].

It is possible to classify this kind of electrical machine into two general groups, if the back-electromagnetic force (EMF) shape is considered: sinusoidal and non-sinusoidal machines. The latter are machines which present different types of back-EMF shape, other than sinusoidal shape, and most common types are the trapezoidal wave shape followed by the square wave shape [3].

The sinusoidal machines are built with windings distributed sinusoidally around the stator to produce a sinusoidal back-EMF wave shape. This is also possible with a pseud-sinusoidal distribution combined with a proper magnetization of rotor magnets. On the other hand, non-sinusoidal machines are simpler than sinusoidal ones, due to a simpler stator winding and a constant magnetization of rotor magnets. This fact is responsible for two major effects: non-sinusoidal machines can have a lower cost than their sinusoidal counterparts and a higher power/weight relation [2,3]. It is common to denote this kind of machine together with its power converter by “brushless DC motor” (BLDC motor) [4,5].

In the same way, sinusoidal machines together with their power converter are denoted by “brushless AC motor” (BLAC motor) [6]. They are used in high-precision positioning systems, due to their low

^{*}Correspondence to: J. R. B. A. Monteiro, Department of Electrical Engineering, School of Engineering of São Carlos (EESC), University of São Paulo (USP), São Carlos, SP 13566-590, Brazil.

[†]E-mail: jrm@sc.usp.br

electromagnetic torque ripple (about 2–8%, depending on the machine, against 7–30% of BLDC motors [7]). These characteristics are a limitation for high-performance and high-precision BLDC motor systems application, therefore such systems commonly employ a BLAC motor [4].

The power converter which is commonly used in BLDC motors is the traditional tri-phase inverter in six-step 120° mode of operation, and its frequency is locked with electrical rotor frequency (the state of any inverter bridge transistor is rotor-position dependent). Therefore, the inverter acts as an “electronic commutator” [2]. Considering only the electrical machine, i.e., the mechanical rotating element of a BLDC motor, it consists of a surface-mount permanent magnet synchronous machine, with a non-sinusoidal back-EMF waveform, more commonly a trapezoidal or square waveform [3,8].

More often, SM-PMSM used in BLDC motors are considered to have a trapezoidal back-EMF waveform, so control strategies are used in order for squarewave stator current to be produced in stator windings (Figure 1). Therefore, PWM current regulators or hysteresis current regulators are used to produce a rectangular stator current pattern [4,5].

There is a wide range of methods for electromagnetic torque ripple reduction in BLDC motors, where their electrical machines are commonly an SM-PMSM with trapezoidal back-EMF waveform [9–12]. For example, in Ref. [13], a machine with a non-ideal trapezoidal waveform is considered and its asymmetries are treated. An equivalent method is also explained in Ref. [9].

There are waveforms that are different from the trapezoidal one presented by SM-PMSMs. Some other wave shapes can be found in Refs. [2,3,14,15].

The main objective of this work is to present a variation of dq transformation, called here “ dq_x transformation,” which is an extension of the classical dq transformation. It can be applied to SM-PMSM with any type of back-EMF waveform and not only to sinusoidal, trapezoidal, or squarewave machines. The resulting mathematical machine model differs from the model shown in Ref. [14], as it presents a new coordinate system of axes that is superposed to the classical dq axes. These new axes are called “ dq_x axes.” They have both a different angle and magnitude from dq axis. This new coordinate system permits writing the electromagnetic torque equation as being directly proportional to the quadrature projected stator current, which is also the same of the sinusoidal electromagnetic torque

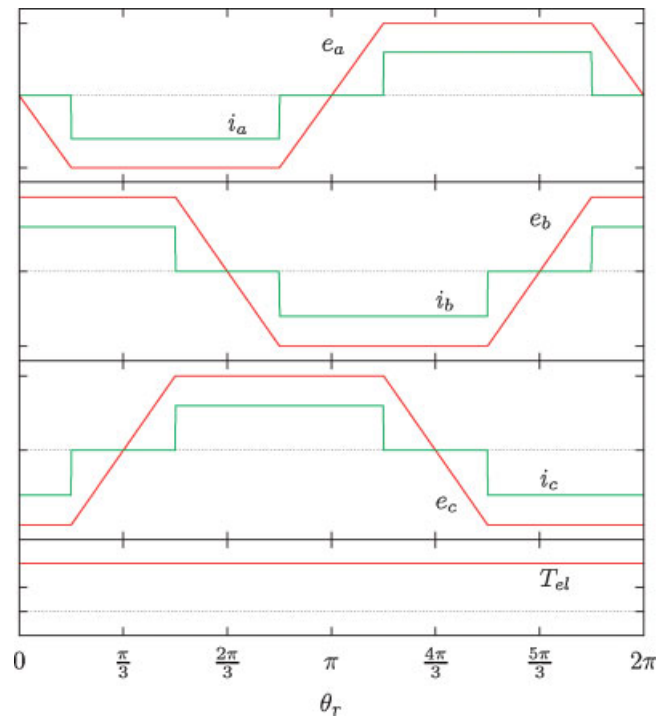


Figure 1. Ideal electromagnetic torque, back-EMF, and phase current waveforms for a SM-PMSM motor.

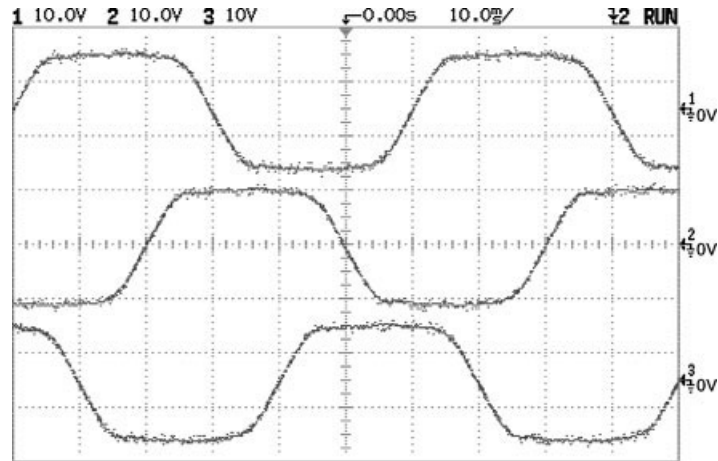


Figure 2. Measured back-EMF wave shapes of a non-sinusoidal SM-PMSM, which are approximately as trapezoidal as in Figure 1. Channel 1: e_a ; channel 2: e_b ; channel 3: e_c .

equation, except for the fact that this equation for sinusoidal machines is written over dq axes and not over dq_x axes, as is the case of non-sinusoidal ones. This model has already been shown in a short form in Refs. [16,17], but here, it is shown in details together with the results of its practical implementation as well as of its simulation.

The used machine for implementation have the back-EMF waveform shown in Figure 2. It can be seen that its back-EMF waveform is not purely trapezoidal, as it was desired like Figure 1. The stator windings are full pitch coils arranged in 60 electrical degrees span, with 3 slots per pole per phase [3].

Section 2 shows a general vectorial model that can be applied to SM-PMSM with any type of back-EMF waveform. Using this model and considering a perfectly sinusoidal back-EMF machine, the vectorial model for sinusoidal machines is shown in Section 3. This section is included here only for comparison purposes, the electromagnetic torque equation of sinusoidal machines is used only as a reference to the deduction of a similar electromagnetic torque equation for non-sinusoidal machines.

Finally, Section 4 displays a specific vectorial model for non-sinusoidal back-EMF machines, which is obtained using the proposed dq_x transformation. This section also shows the expression for electromagnetic torque, and the torque equation is written as being directly proportional to the direct component of the stator current, in dq_x coordinate axes, which is equivalent to the same equation for sinusoidal machines. It is possible to apply the vectorial model shown in Section 4 in a drive system without machine stator current measurement, it is shown in Section 5. In Section 7, practical results of a real positioning system with the implemented vectorial model are shown. Eventually, these results are compared to the same machine driven by the classical six-step 120°. Once the proposed vectorial model permits the application of vectorial control without the necessity of measuring the stator phase currents, the application of both methods differs only by the use of a microcontroller.

2. GENERAL VECTORIAL MODEL

For the development of all SM-PMSM model equations, the following hypotheses are considered together with the schematic diagram shown in Figure 3 [18]:

- the machine is a symmetrical tri-phase machine;
- the variation of reluctance of rotor magnetic circuit, due to the rotor position, is not worthy of notice;
- there is no saturation in iron, considering the machine's normal operating region.

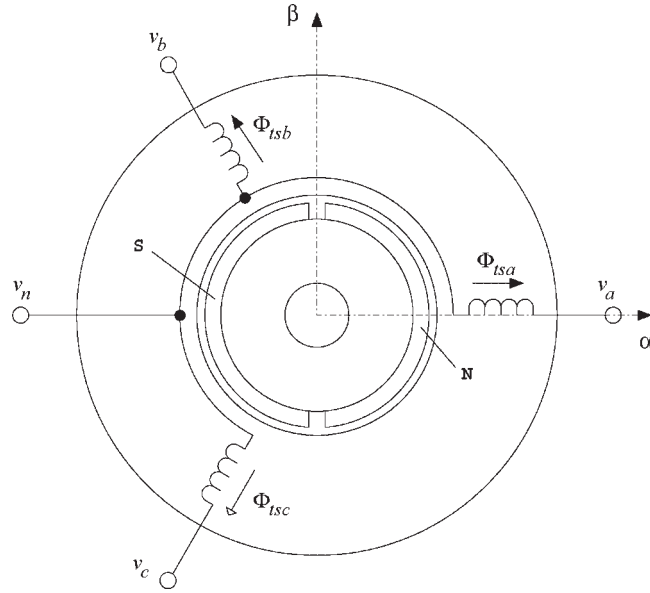


Figure 3. Schematic diagram of a surface-mount permanent-magnet synchronous machine.

Considering such hypotheses and Figure 3, phase voltages, the back-EMF waveform of each phase and the machine's electromagnetic torque are given by (1), (2) and (3), respectively. Regarding such equation deductions, they can be found in literature [18].

$$\begin{bmatrix} u_a \\ u_b \\ u_c \end{bmatrix} = \begin{bmatrix} L_s & M_s & M_s \\ M_s & L_s & M_s \\ M_s & M_s & L_s \end{bmatrix} \frac{d}{dt} \begin{bmatrix} i_a \\ i_b \\ i_c \end{bmatrix} + R_s \begin{bmatrix} i_a \\ i_b \\ i_c \end{bmatrix} + \begin{bmatrix} e_a \\ e_b \\ e_c \end{bmatrix} + \begin{bmatrix} u_n \\ u_n \\ u_n \end{bmatrix} \quad (1)$$

where e_a , e_b , and e_c : induced voltage of stator phases a, b, and c, respectively, due to rotor magnets movement, as in Equation (2); i_a , i_b , and i_c : stator phase currents a, b, and c, respectively; L_s : stator phase self-inductance; M_s : stator phases mutual inductances; R_s : stator phase resistance; u_a , u_b , and u_c : a, b, and c stator phases applied voltages, respectively (Figure 3); u_n : stator neutral terminal voltage (this terminal is not normally connected, Figure 3).

$$\begin{bmatrix} e_a \\ e_b \\ e_c \end{bmatrix} = \frac{d}{dt} \begin{bmatrix} \Phi_{ra} \\ \Phi_{rb} \\ \Phi_{rc} \end{bmatrix} = \omega_r \begin{bmatrix} \Phi'_{ra} \\ \Phi'_{rb} \\ \Phi'_{rc} \end{bmatrix} \quad (2)$$

where Φ_{ra} , Φ_{rb} , and Φ_{rc} : linked magnetic fluxes between rotor magnets and stator winding phases a, b, and c, respectively; ω_r : electrical rotor speed.

$$T_{el} = n_{pp} (\Phi'_{ra} i_a + \Phi'_{rb} i_b + \Phi'_{rc} i_c) \quad (3)$$

where T_{el} : machine-generated electromagnetic torque; n_{pp} : number of machine's pole pairs.

From (2), it is possible to derive:

$$\begin{bmatrix} \Phi'_{ra} \\ \Phi'_{rb} \\ \Phi'_{rc} \end{bmatrix} = \frac{1}{\omega_r} \frac{d}{dt} \begin{bmatrix} \Phi_{ra} \\ \Phi_{rb} \\ \Phi_{rc} \end{bmatrix} \quad (4)$$

Applying $\alpha\beta\theta$ transformation, as given by (5) and (6), to (1), (2), and (3), the electrical machine equations are obtained, (7) and (8), as well as the electromagnetic torque equation, (9), in the

coordinate axes $\alpha\beta 0$.

$$x_{\alpha\beta} = \sqrt{\frac{2}{3}} \begin{bmatrix} 1 & e^{j\frac{2\pi}{3}} & e^{-j\frac{2\pi}{3}} \end{bmatrix} \begin{bmatrix} x_a \\ x_b \\ x_c \end{bmatrix} \quad (5)$$

$$x_0 = \sqrt{\frac{2}{3}} \begin{bmatrix} \frac{\sqrt{2}}{2} & \frac{\sqrt{2}}{2} & \frac{\sqrt{2}}{2} \end{bmatrix} \begin{bmatrix} x_a \\ x_b \\ x_c \end{bmatrix} \quad (6)$$

$$u_{\alpha\beta} = R_s i_{\alpha\beta} + (L_s - M_s) \frac{d}{dt} i_{\alpha\beta} + \omega_r \Phi'_{r\alpha\beta} \quad (7)$$

$$u_0 = R_s i_0 + (L_s + 2M_s) \frac{d}{dt} i_0 + \frac{\sqrt{3}}{3} u_n \quad (8)$$

$$T_{el} = n_{pp} (\Phi'_{r\alpha} i_\alpha + \Phi'_{r\beta} i_\beta + \Phi'_{r0} i_0) \quad (9)$$

where $x_{\alpha\beta}$: quantities written over $\alpha\beta$ axes (complex number); x_0 : zero component; x_a , x_b , and x_c : quantities of a, b, and c phases, respectively.

The machine equations in dq_x coordinate axes are obtained by applying the dq_x transformation (10) to (7) and (9). The zero component will not be considered from this point as the neutral terminal connection is not used, as is most cases, so $i_0 = 0$.

$$x_{\alpha\beta} = a_x e^{j\theta_x} e^{j\theta_r} x_{dq_x} \quad (10)$$

where a_x : dq_x size of axes, relatively to dq axes, which are considered equal to the unity (Figure 5); θ_x : angle of dq_x axes, relatively to dq axes (Figure 5).

The dq_x transformation is presented in Figure 4 for a better understanding. This transformation can be decomposed into two ordinary transformations: a dq transformation, with its angle equal to the machine's electrical rotor angle (θ_r), followed by another transformation composed of a pair of orthogonal axes of an arbitrary size a_x and an arbitrary angle θ_x , in relation to the dq axes. In that figure, x_{dq_x} stands for quantities in dq_x axes.

The relations between $\alpha\beta$, dq , and dq_x axes are shown in Figure 5. It is also observed that dq_x transformation consists of a new axes rotation (θ_x rotation), and a resize of a_x , since dq and $\alpha\beta$ axes magnitudes are equal to unity. Therefore, the new dq_x axes are orthogonal and have a variable length and angle as a function of electrical rotor angle (θ_r).

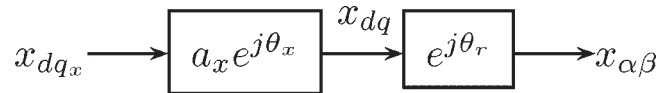


Figure 4. dq_x transformation represented by blocks.

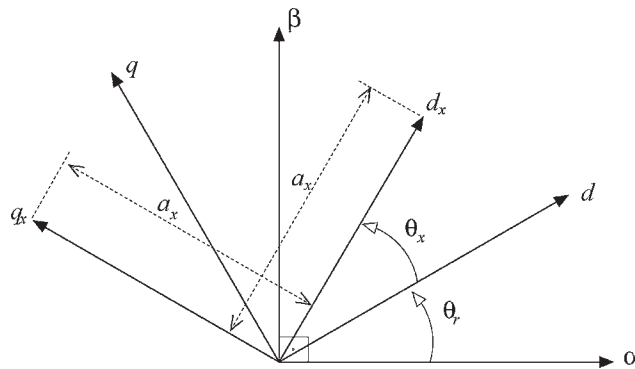


Figure 5. Relation between $\alpha\beta$, dq , and dq_x coordinate axes.

The relation between only dq and dq_x axes is shown by (11).

$$x_{dq} = a_x e^{j\theta_x} x_{dq_x} \quad (11)$$

By the application of dq_x transformation (10) in the machine's electrical (7) and electromagnetic torque (9) equations, the same equations for dq_x axes are obtained, (12) and (13).

$$\begin{aligned} u_{dq_x} &= R_s i_{dq_x} + (L_s - M_s) \frac{d}{dt} i_{dq_x} + \\ &(L_s - M_s) \omega_r i_{dq_x} \left(\frac{a'_x}{a_x} + j(1 + \theta'_x) \right) + \\ &\omega_r \Phi'_{rdq_x} \end{aligned} \quad (12)$$

$$T_{el} = n_{pp} a_x^2 \left(i_{d_x} \Phi'_{rd_x} + i_{q_x} \Phi'_{rq_x} \right) \quad (13)$$

where

$$a'_x = \frac{da_x}{d\theta_r} \quad (14)$$

$$\theta'_x = \frac{d\theta_x}{d\theta_r} \quad (15)$$

3. SINUSOIDAL MACHINE VECTORIAL MODEL

The vectorial model for a sinusoidal SM-PMSM is obtained by considering the magnetic fluxes linked with a stator phase and rotor magnets, given by (17) and applying dq transformation (16) to (1) and (3), which is equivalent to (10) with $a_x = 1$ and $\theta_x = 0$. Considering the dq axes angle (Figure 5) equal to rotor angle (θ_r), equations (18)–(21) are obtained.

$$x_{\alpha\beta} = e^{j\theta_r} x_{dq} \quad (16)$$

where x_{dq} : dq axes quantities, as a complex number; θ_{dq} : dq axes angle (arbitrary value).

$$\begin{bmatrix} \Phi_{ra} \\ \Phi_{rb} \\ \Phi_{rc} \end{bmatrix} = \Phi_m \begin{bmatrix} \cos\theta_r \\ \cos(\theta_r - \frac{2\pi}{3}) \\ \cos(\theta_r + \frac{2\pi}{3}) \end{bmatrix} \quad (17)$$

where Φ_m : maximum value of magnetic fluxes linked with a stator phase produced only by rotor magnets.

$$\Phi'_{rd} = 0 \quad (18)$$

$$\Phi'_{rq} = \sqrt{\frac{3}{2}} \Phi_m \quad (19)$$

$$\begin{aligned} u_{dq} &= R_s i_{dq} + (L_s - M_s) \frac{d}{dt} i_{dq} \\ &+ j(L_s - M_s) \omega_r i_{dq} + j\omega_r \sqrt{\frac{3}{2}} \Phi_m \end{aligned} \quad (20)$$

$$T_{el} = n_{pp} \sqrt{\frac{3}{2}} \Phi_m i_q \quad (21)$$

The main characteristic of the vectorial sinusoidal model is seen in Equation (21): the produced electromagnetic torque is directly proportional to the quadrature component of stator current (i_q). This

is due to the fact that the magnetic flux projected in direct axis (d) is constant while the one projected in quadrature axis (q) is null, so Φ'_{rd} is null and Φ'_{rq} is constant, (18) and (19).

4. NON-SINUSOIDAL MACHINE VECTORIAL MODEL

For a non-sinusoidal SM-PMSM model, the electromagnetic torque equation is desired to be as simple as the one for sinusoidal machine (21). Thus, similarly to the sinusoidal machine (although over dq_x axes), there is a condition where Φ'_{rd_x} is null. This condition is given by (22) and (23), which are derived from (13) and (21).

Sinusoidal (trapezoidal)

$$\Phi'_{rd_x} = 0 \quad (22)$$

$$a_x^2 \Phi'_{rq_x} = \sqrt{\frac{3}{2}} \Phi_m \quad (23)$$

If the above conditions are satisfied, the electromagnetic torque equation for any type of machine, i.e., with any type of back-EMF wave shape, is written by (24).

$$T_{el} = n_{pp} \sqrt{\frac{3}{2}} \Phi_m i_{q_x} \quad (24)$$

By (24), the electromagnetic torque is directly proportional to the stator current projected in q_x axis, which is similar to the same equation for sinusoidal machine, except for the fact that the q axis current projection is used there (21). For (24) to be possible, a_x and θ_x must be defined by (25) and (26).¹

$$a_x = \sqrt{\frac{3}{2}} \frac{\Phi_m}{\sqrt{\Phi_{r\alpha}^{\prime 2} + \Phi_{r\beta}^{\prime 2}}} \quad (25)$$

$$\theta_x = \tan^{-1} \frac{-\Phi'_{r\alpha}}{\Phi'_{r\beta}} - \theta_r \quad (26)$$

Such results also show that if a classical dq transformation, without any modification, is applied to a non-sinusoidal SM-PMSM, this machine will present harmonic components in its electromagnetic torque, as in non-sinusoidal back-EMF waveforms, $\theta_x = 0$ and $a_x = 1$ are not valid.

Using (11), (20), (25), and (26), the electric machine equation in complex form (27) is obtained for any type of back-EMF waveform.

$$\begin{aligned} u_{dq_x} = & R_s i_{dq_x} + (L_s - M_s) \frac{di_{dq_x}}{dt} + \\ & (L_s - M_s) \left(\omega_r i_{dq_x} \left(\frac{a_x'}{a_x} + j(1 + \theta_x') \right) \right) + \\ & j \sqrt{\frac{3}{2}} \Phi_m \frac{1}{a_x'} \omega_r \end{aligned} \quad (27)$$

Considering different back-EMF wave shapes, there will be different values for a_x and θ_x , remembering that both are functions of electrical rotor angle θ_r .

For a perfect trapezoidal back-EMF, a_x and θ_x are shown in Figure 6. In Figure 7, a_x and θ_x are shown for back-EMF waveforms of Figure 2.

¹See Appendix for equation deductions.

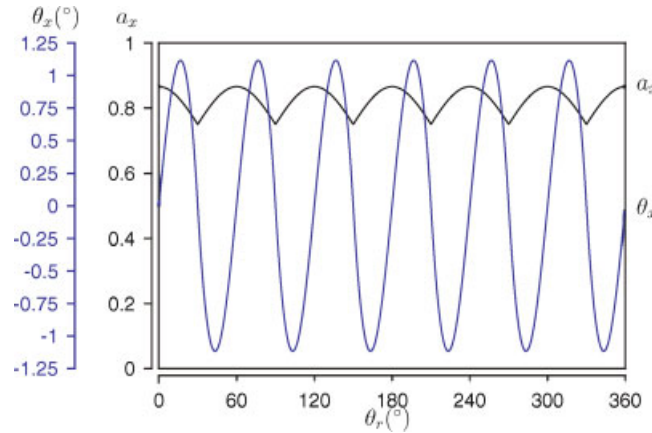


Figure 6. Parameters $a_x(\theta_r)$ and $\theta_x(\theta_r)$ for an ideal trapezoidal back-EMF waveform (θ_r and θ_x in electrical degrees).

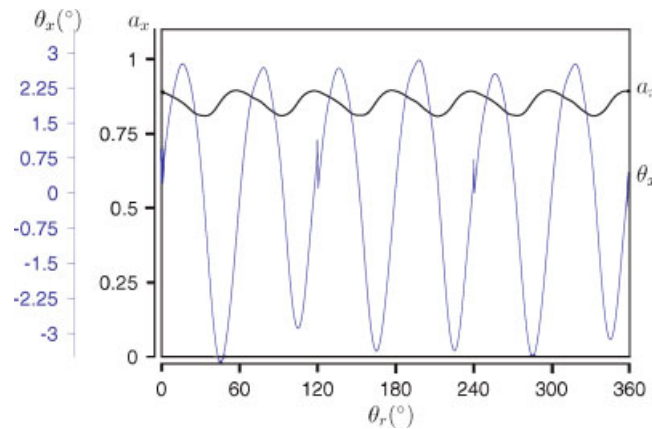


Figure 7. Parameters $a_x(\theta_r)$ and $\theta_x(\theta_r)$ for a back-EMF waveform as presented in Figure 2 (θ_r and θ_x in electrical degrees).

5. CURRENT OPEN-LOOP VECTORIAL CONTROL

This section shows that it is possible to apply the proposed vectorial control without the need of stator current measurement. The model equations are manipulated to allow it. The resulting control system relies in the previous knowledge of machine parameters as stator resistance, inductances, and back-EMF waveforms. The resulting control block for this current open-loop control is shown in Figure 8.

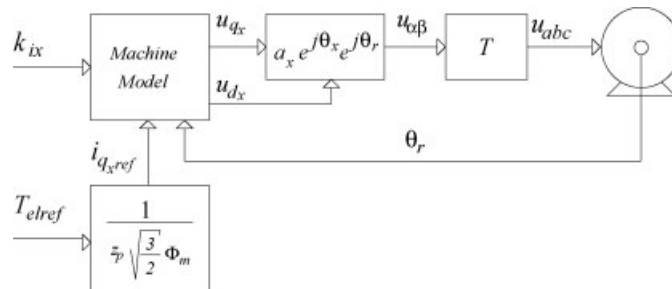


Figure 8. Block diagram of a BLDC motor drive system, using the control based on the vectorial model, in stator current open-loop.

The obtained non-sinusoidal SM-PMSM electrical equation is more complex than the sinusoidal one, (20) and (27), but the electromagnetic torque equation for non-sinusoidal machine (24) is as simple as the one for sinusoidal machine (21). In order to produce a ripple free electromagnetic torque, it is necessary to keep i_{q_x} constant, therefore di_{q_x}/dt must be equal to zero.

In the case of a control system for machine electromagnetic torque, using (24),

$$i_{q_x,ref} = T_{elref} \sqrt{\frac{2}{3}} \frac{1}{n_{pp} \Phi_m} \quad (28)$$

where T_{elref} is the reference for machine electromagnetic torque and $i_{q_x,ref}$ is the reference current for q_x axis projected stator current component.

If i_{d_x} is held constant, too, di_{d_x}/dt must be zero and it is possible to write $i_{d_x,ref}$ (project d_x axis reference stator current component) as proportional to $i_{q_x,ref}$:

$$i_{d_x,ref} = k_{ix} i_{q_x,ref} \quad (29)$$

where k_{ix} is constant and limited to the interval $[-1, 1]$. For negative values of k_{ix} , the machine is under field weakening and, for positive values, the machine is under field enhancement. For $k_{ix} = 0$, the copper loss is at its minimum value, as only the portion of current which is responsible for torque production is applied to the stator.

Considering $i_{q_x} = i_{q_x,ref}$ and $i_{d_x} = i_{d_x,ref}$, the electrical machine equations are written as follows:

$$u_{d_x} = \left(R_s k_{ix} + (L_s - M_s) \omega_r \left(\frac{a'_x}{a_x} k_{ix} - (1 + \theta'_x) \right) \right) i_{q_x,ref} \quad (30)$$

$$u_{q_x} = \left(R_s + (L_s - M_s) \omega_r \left(\frac{a_x}{a'_x} + (1 + \theta_x) k_{ix} \right) \right) i_{q_x,ref} + \sqrt{\frac{3}{2}} \Phi_m \frac{1}{a_x^2} \omega_r \quad (31)$$

By observing (28)–(31), it is not necessary to measure the stator currents, so the employment of current sensors, signal isolators and analog-to-digital converters is not necessary either. Those equations are not part of transformations, they consist of an integrated controller and estimator for stator currents. Electric drive positioning systems usually have high-resolution optical encoders for rotor position sensing, so there is no need to use additional components to the system, except for a higher capacity processor, whether all machine parameters are known.

Figure 8 shows a control block diagram of the complete drive system. The diagram is a stator current open-loop control, so it refers to Equations (30) and (31). All the system works in an open-loop control, since all machine parameters are known. The reference torque is used to determine the reference current in q_x axes by (24) and using (24) and (12), u_{d_x} and u_{q_x} are determined. Parameters a_x and θ_x are determined by (26) and (25), in Section 4. These quantities, which are projected in dq_x axes, are then transformed to $\alpha\beta$ axes, by (10), and then to u_a , u_b , and u_c , using (5). In Figure 8, the “T” block corresponds to the inverse of $\alpha\beta 0$ transformation, (5) and (6), and “Machine Model” block corresponds to (30) and (31).

6. CURRENT CLOSED-LOOP VECTORIAL CONTROL

Considering a control system where stator phase currents are directly measured by current transducers (Figure 9), since there are no need of stator current estimation, the computation time will be reduced, if compared to the current open-loop schema which needs (28)–(31). In that Figure, dq_x to $\alpha\beta$ and $\alpha\beta$ to abc transformations will be necessary in order to transform the applied stator voltage from dq_x axes to abc . Also, the inverse of those transformations will be necessary to transform stator currents from abc to dq_x axes.

The use of current transducers will allow a slower processor, if compared to the current open-loop schema, and also will improve electromagnetic torque transient response. It is possible to use three (one for each stator phase) or two current sensors. In the last case, the third current phase will be given by

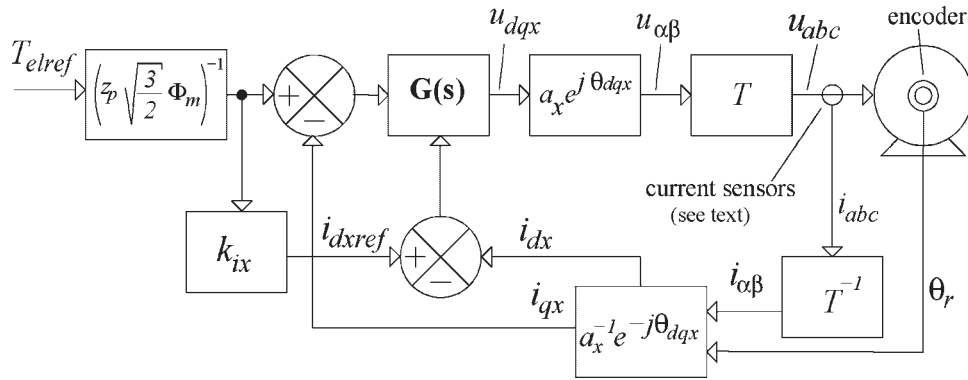


Figure 9. Block diagram of a BLDC motor drive system, using the control based on the vectorial model, with current sensors (stator current closed-loop). Note that $\theta_{dqx} = \theta_r + \theta_x$.

(32), once neutral connection is not used. Figure also shows d_x current component control loop. It can be used as field weakening/enhancement or, for copper losses minimization, k_{ix} can be set to 0 (and consequently $i_{dx} = 0$; Section 8). Figure also shows $G(s)$ as a generic controller and it consists of a system of two inputs and two outputs (u_{dx} and u_{qx}). There are several possibilities for the controller topology, from simple classical control topologies to intelligent algorithms.

$$i_a + i_b + i_c = 0 \tag{32}$$

7. BLDC MOTOR DRIVE SYSTEM IMPLEMENTATION USING VECTORIAL MODEL

The block diagram of the hardware used for the implementation of BLDC motor drive is shown in Figure 10. This hardware was used for both classical six-step 120° and control based on vectorial model implementation, in stator current open-loop control, as described in Section 5 (Figure 8). The microcontroller used has an ARM7TDMI core. The optical encoder for rotor position sensing has 10 bits of resolution. The parameters of the used SM-PMSM machine are shown in Table I and its back-EMF waveform is in Figure 2. The control software was entirely developed in a GNU/Linux environment, using C language (GCC configured as a cross compiler).

Some results obtained from implementation are shown in Figures 11 and 12, where one-stator phase current of BLDC motor is presented. The PWM frequency switching is 6 kHz and the electrical power converter fed the machine in current open-loop, as in Section 5. In Figure 11, the machine's

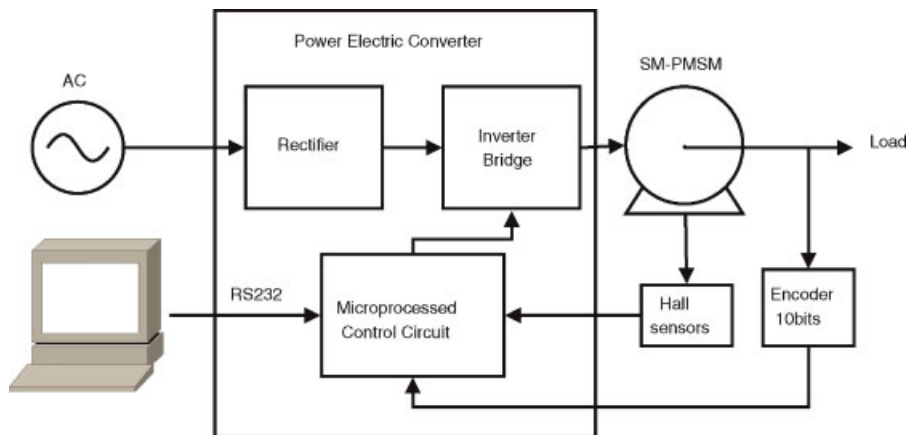


Figure 10. Schematic diagram of hardware used for BLDC motor drive system.

Table I. BLDC motor parameters used in this work.

Parameter	Value	Units
R_s	2.3	Ω
$(L_s - M_s)$	12.5	mH
n_{pp}	3	
Φ_m	0.12	Wb

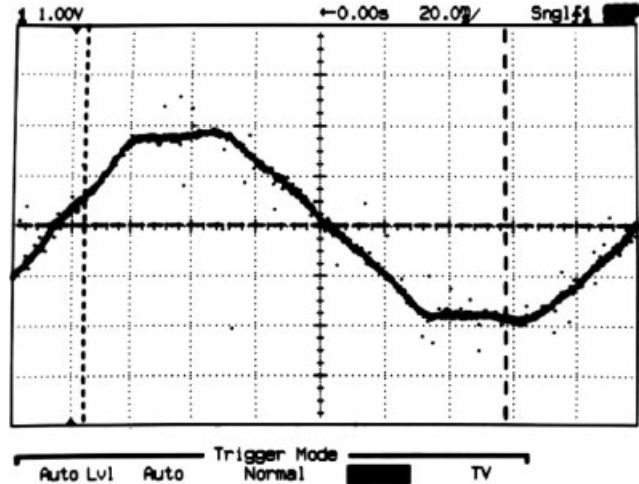


Figure 11. Stator phase current for SM-PMSM with its electric power converter employing control based on the presented vectorial model (current: 2.13 A/div, $\omega_m = 107.9$ rpm, $T_{el} = 2.0$ Nm).

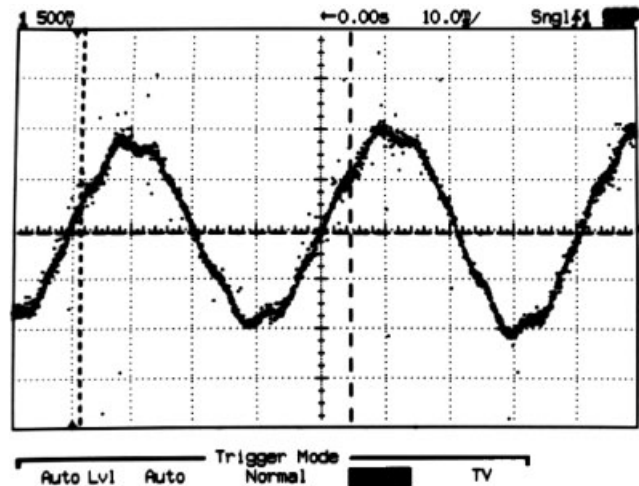


Figure 12. Stator phase current for SM-PMSM with control based on the vectorial model (current: 1.06 A/div, $\omega_m = 645.6$ rpm, $T_{el} = 1.2$ Nm).

electromagnetic torque is about 2 Nm and the mechanical rotor speed is about 11.3 rd/second (107.9 rpm). In Figure 12, the machine's electromagnetic torque is about 1.2 Nm and the mechanical rotor speed is about 67.6 rd/second (645.6 rpm).

The performance of a positioning drive system, using a BLDC motor with its electrical converter based on the presented vectorial model, and another drive system, using a BLDC motor with classical six-step 120° electric power converter, was analyzed.

The simplified block diagrams for each system are shown in Figures 13 and 14. The former refers to the conventional BLDC motor, using conventional six-step 120° power converter and the latter refers to BLDC motor with power converter using control based on the non-sinusoidal vectorial model. Both systems were tested under the same operational conditions and in stator current open-loop, i.e., with no current measurement in both cases.

The results for mechanical rotor position (θ_m) are shown in Figures 15–17, for six-step mode of operation, and in Figures 18–20, for the vectorial mode of operation. According to those figures, by using the presented vectorial model, it is possible to significantly reduce the ripple in rotor position, due to the ripple reduction in rotor electromagnetic torque. Figures also show a interesting result regarding cogging torque. This machine has 36 slots in its stator, and was constructed employing some techniques in order to minimize cogging torque as skewing and and reasonably small stator slots openings [2,3,9]. So, if cogging torque was a significant source of ripple for this machine, a position disturbance in each 10 electrical degrees (3.33 mechanical degrees) would be expected.

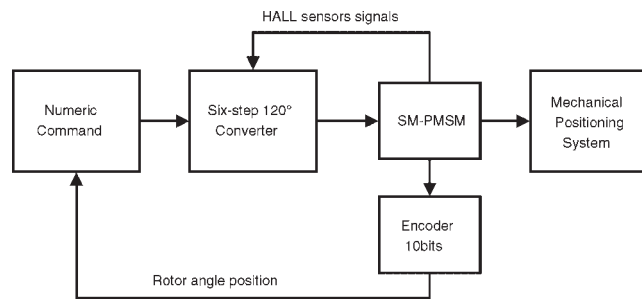


Figure 13. Simplified block diagram for conventional six-step 120° BLDC motor electric power converter.

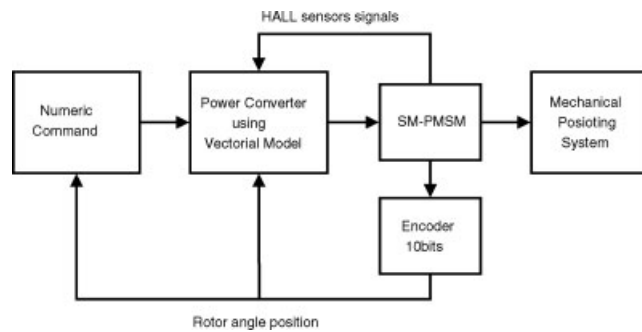


Figure 14. Simplified block diagram for BLDC motor with electric power converter using the vectorial model.

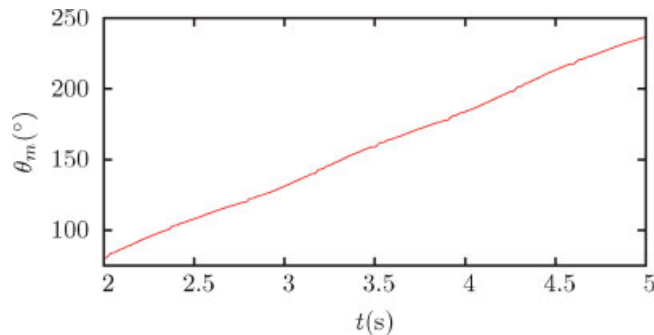


Figure 15. Mechanical angular rotor position for a positioning drive system using BLDC motor with conventional six-step 120° electric power converter.

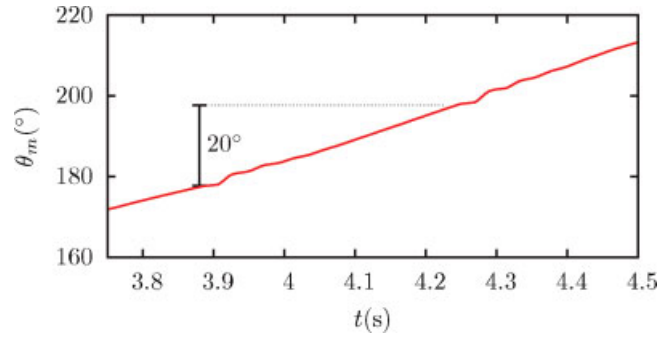


Figure 16. Figure 15 zoomed. It can be seen, by machine position, that torque ripple occurs each 20 mechanical degrees, or 60 electrical degrees.

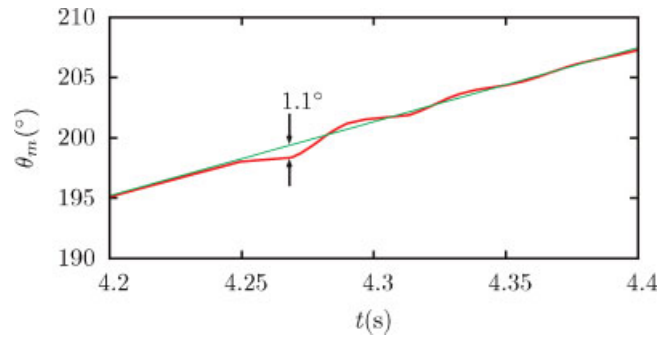


Figure 17. Figure 16 zoomed, for position ripple detail, due to machine produced torque ripple.

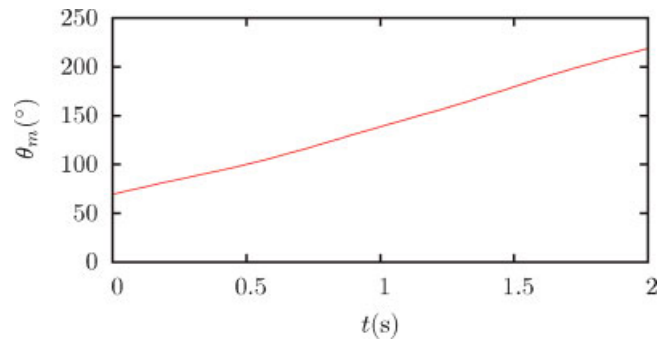


Figure 18. Angular rotor position for a positioning drive system using BLDC motor with electric power converter employing control based on the presented vectorial model.

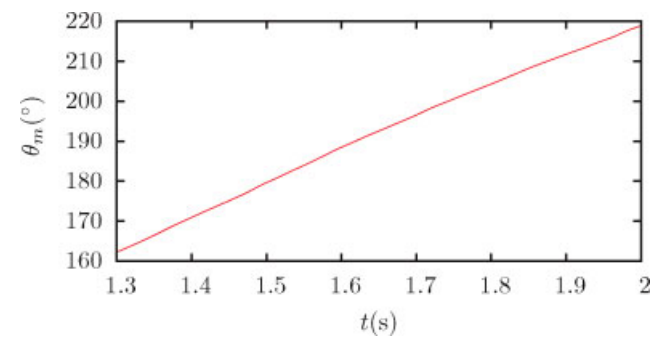


Figure 19. Figure 18 zoomed, as Figure 16 is from Figure 15.

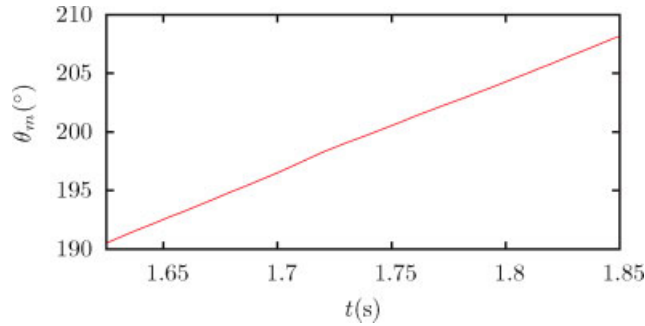


Figure 20. Figure 19 zoomed, for position ripple detail, like Figure 17 is from Figure 16.

8. STATOR COPPER LOSSES

With respect to copper losses, it is possible to minimize it by controlling i_{dx} current component, once it is only i_{qx} current component that produces electromagnetic torque, according to (24). Figure 21 shows ideal squarewave current for one stator phase together with its projections on dq_x axes, direct (i_{dx}) and quadrature (i_{qx}) components.

Figure 22 shows the stator current which is the resulting of current i_{qx} of Figure 21 with its d_x component equal to zero. Also, for comparison purposes, the ideal squarewave is shown. Both stator

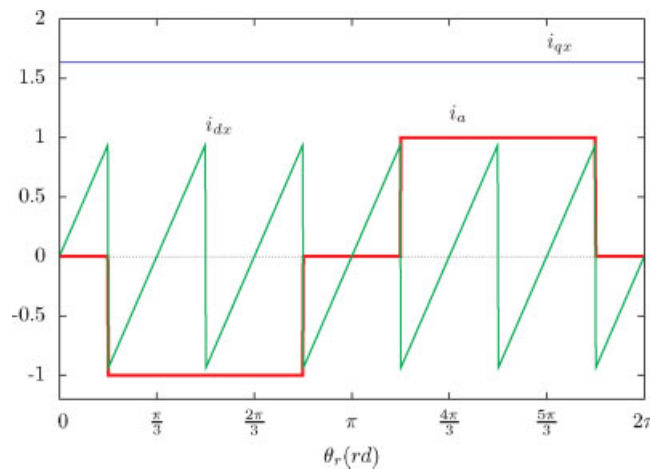


Figure 21. Ideal squarewave stator phase current and its d_x and q_x components as a function of rotor position.

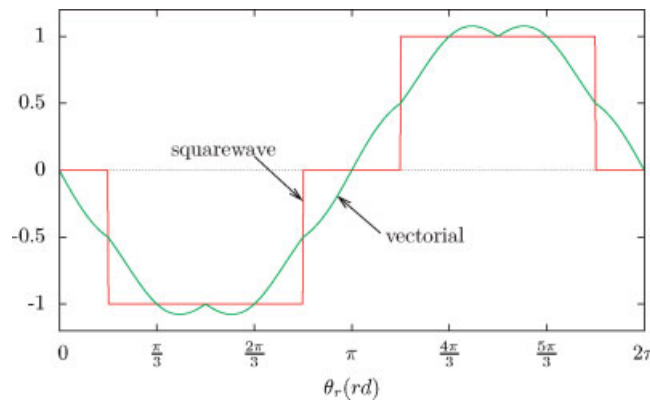


Figure 22. Ideal squarewave stator phase current and stator phase current that produces the same electromagnetic torque but with no d_x component.

Table II. RMS values for stator phase current waveforms of Figure 22.

Waveform	RMS value	Unit
Squarewave	$\sqrt{\frac{2}{3}} = 0.816496 \dots$	A
Vectorial	$0.777722 \pm 5.10 \times 10^{-6}$	A

currents produce a constant electromagnetic torque (in an ideal situation), with no ripple, although they are quite different. Also, they have distinct RMS values, as shown in Table II.

As copper losses are given by (33) and squarewave RMS value is greater than vectorial waveform RMS value, the copper losses for the vectorial waveform is lower than for square waveform current. Thus, considering an ideal SM-PMSM with ideal trapezoidal back-EMF waveforms, if a square current waveform, such as shown in Figure 21, is applied in its stator phases, its copper losses will be 10.2% higher than the same machine with vectorial current waveforms in its stator phases, producing the same electromagnetic torque in both cases.

$$P_{Cu} = 3R_s I_{RMS}^2 \quad (33)$$

where I_{RMS} is the RMS current value for one phase.

Nonetheless, it is important to point out that in practice, it is very hard to produce an ideal squarewave stator current, due to its high di/dt values, and also, back-EMF waveform is not a pure trapezoidal function. Those facts cause stator copper losses to be even higher than vectorial case, once it is possible to produce stator currents like the vectorial waveform of Figure 22, and in the case of back-EMF distortions, it is even possible to produce an adapted stator current waveform for that kind of machine, with a specific back-EMF waveform.

9. CONCLUSIONS

A vectorial model for surface-mount permanent magnet synchronous machines has been presented in this work, obtained by using an extension of dq transformation, called here by “ dq_x transformation,” It allows applying vectorial control to SM-PMSM with any type of back-EMF waveform. Practical results have shown the model can improve the machine’s performance, reducing its electromagnetic torque ripple and copper losses, in comparison to the conventional use of classical six-step 120° electric power converter, commonly applied to this type of machines. This performance improvement is achieved even in open-loop current control, as in the six-step converter case.

The use of dq_x transformation allows for the application of vectorial control to non-sinusoidal SM-PMSMs (any type of back-EMF waveforms), without the need of measuring stator currents. Considering the positioning drive systems using conventional BLDC motors (composed of SM-PMSM with electrical power converter in six-step operation mode) coupled with an optical encoder for rotor angle measurement, the difference between the hardware used in this case and the hardware used in the case of vectorial model consists only in the processor used for the vectorial control implementation. Although vectorial control can be implemented without the need of stator current measurement, with stator current information, the system performance can be highly increased, i.e., dynamical electromagnetic torque response is increased, and there is no need of some machine parameters: stator resistance (R_s), self and mutual inductances ($L_s - M_s$).

Also considering positioning systems, they must have acceptable performance mainly at lower speed operation, where they must have a low level of electromagnetic torque ripple. At high operation speed, the torque ripple produced by the machine is filtered by the inertia of the mechanical system. Nonetheless, even at high speed operation, the control based on the presented vectorial model allows for a low electromagnetic torque ripple. The stator phase current does not require high values of di/dt to

produce smooth electromagnetic torque, so with the same inverter bus voltage, the squarewave current path is harder to obtain than the vectorial current path (Figures 21 and 22).

As well as for positioning systems applications, the vectorial method also shows to be valuable for traction applications, due to its better energy efficiency, i.e., it allows a reduction in stator copper losses.

10. LIST OF SYMBOLS

a_x	dq_x size of axes, relatively to dq axes, which are considered equal to the unity (Figure 5)
$e_a, e_b,$ and e_c	induced voltage of stator phases a, b, and c, respectively, due to rotor magnets movement, as in Equation (2)
G(s)	generic multiple input, multiple output controller
$i_a, i_b,$ and i_c	stator phase currents a, b, and c, respectively
i_{dq}	stator phase currents projected in dq axes (in complex form: $i_d + ji_q$)
i_{dq_x}	stator phase currents projected in dq_x axes (in complex form: $i_{d_x} + ji_{q_x}$)
$i_{d_x\text{ref}}$	is the reference current for d_x axis projected stator current component
$i_{q_x\text{ref}}$	is the reference current for q_x axis projected stator current component
I_{RMS}	RMS current value for one stator phase
$i_{\alpha\beta}$	stator currents in $\alpha\beta$ axes (in complex form: $i_\alpha + ji_\beta$)
k_{is}	flux enhancing/weakening constant
L_s	stator phase self-inductance
M_s	stator phases mutual inductances
n_{pp}	number of machine's pole pairs
P_{Cu}	total stator copper losses
R_s	stator phase resistance
T	$\alpha\beta 0$ to abc matrix transformation
T_{el}	machine-generated electromagnetic torque
T_{elref}	machine electromagnetic torque reference
$u_a, u_b,$ and u_c	a, b, and c stator phases applied voltages, respectively (Figure 3)
u_{dq}	stator voltages in dq axes (in complex form: $u_d + ju_q$)
u_{dq_x}	stator voltages in dq_x axes (in complex form: $u_{d_x} + ju_{q_x}$)
u_n	stator neutral terminal voltage (this terminal is not normally connected, Figure 3)
$u_{\alpha\beta}$	stator voltages in $\alpha\beta$ axes (in complex form: $u_\alpha + ju_\beta$)
$x_a, x_b,$ and x_c	arbitrary quantities in a, b, and c phases, respectively
x_{dq}	dq axes quantities, as a complex number: $x_d + jx_q$
x_{dq_x}	dq_x axes quantities, as a complex number: $x_{d_x} + jx_{q_x}$
x_0	arbitrary quantity zero component
$x_{\alpha\beta}$	arbitrary quantities written over $\alpha\beta$ axes (complex number)
Φ_m	maximum value of magnetic fluxes linked with a stator phase produced only by rotor magnets
$\Phi_{ra}, \Phi_{rb},$ and Φ_{rc}	linked magnetic fluxes between rotor magnets and stator winding phases a, b, and c, respectively
$\Phi'_{ra}, \Phi'_{rb},$ and Φ'_{rc}	back-EMF waveforms of phases a, b, and c, respectively, due only to rotor magnets
Φ'_{rdq}	back-EMF waveforms due only to rotor magnets, projected in dq axes (complex form: $\Phi'_{rd} + j\Phi'_{rq}$)
Φ'_{rdq_x}	back-EMF waveforms due only to rotor magnets, projected in dq_x axes (complex form: $\Phi'_{rd_x} + j\Phi'_{rq_x}$)
$\Phi'_{r\alpha\beta}$	back-EMF waveforms due only to rotor magnets, projected in $\alpha\beta$ axes (complex form: $\Phi'_{r\alpha} + j\Phi'_{r\beta}$)
θ_{dq}	dq axes angle (arbitrary value)
θ_{dq_x}	dq_x axes angle (arbitrary value)

θ_m	mechanical rotor angle
θ_r	electrical rotor angle
θ_x	angle of dq_x axes, relatively to dq axes (Figure 5)
ω_r	electrical rotor speed

ACKNOWLEDGEMENTS

The authors would like to acknowledge “Fundação de Amparo à Pesquisa do Estado de São Paulo” (FAPESP) and “Conselho Nacional de Desenvolvimento Científico e Tecnológico” (CNPq), for the financial support given to this research.

APPENDIX

This appendix shows how (25) and (26) are obtained.

From (10):

$$a_x \sqrt{\Phi'_{rdx}{}^2 + \Phi'_{rqx}{}^2} = \sqrt{\Phi'_{r\alpha}{}^2 + \Phi'_{r\beta}{}^2} \quad (\text{A.1})$$

As $\Phi'_{rdx} = 0$:

$$a_x \Phi'_{rqx} = \sqrt{\Phi'_{r\alpha}{}^2 + \Phi'_{r\beta}{}^2} \quad (\text{A.2})$$

Substituting (A.2) in (23), (25) is obtained.

In the same way, (26) can be derived from (10):

$$\Phi'_{r\alpha\beta} = a_x e^{j\theta_x} e^{j\theta_r} j \Phi'_{rqx} = a_x e^{j\theta_x} e^{j\theta_r} e^{j\frac{\pi}{2}} \Phi'_{rqx} \quad (\text{A.3})$$

Then:

$$\tan^{-1} \frac{\Phi'_{r\beta}}{\Phi'_{r\alpha}} = \theta_x + \theta_r + \frac{\pi}{2} \quad (\text{A.4})$$

REFERENCES

1. Vagati A, Fratta A, Franceschini G, Rosso P. AC motors for high-performance drivers: A design-based comparison. *IEEE Transactions on Industry Applications* 1996; **32**(5): 1211–1219.
2. Miller TJE. *Bushless Permanent-Magnet and Reluctance Motor Drives*. Claredon Press: Oxford, 1993.
3. Nasar SA, Boldea I, Unnewehr LE. *Permanent Magnet, Reluctance, and Self Synchronous Motors*. CRC Press: Boca Raton, 1993.
4. Pillay P, Krishnan R. Modeling, simulation, and analysis of permanent-magnet motor drives. Part II: The brushless dc motor drive. *IEEE Transactions on Industry Applications* 1989; **25**(2): 274–279.
5. Evans PD, Brown D. Simulation of brushless dc drives. *IEEE Proceedings Pt. B* 1990; **137**(5): 299–308.
6. Pillay P, Krishnan R. Modeling, simulation, and analysis of permanent-magnet motor drives. Part I: The permanent-magnet synchronous motor drive. *IEEE Transactions on Industry Applications* 1989; **25**(2): 265–273.
7. Holtz J, Springob L. Identification and compensation of torque ripple in high precision permanent magnet motor drives. *IEEE Transactions on Industrial Electronics* 1996; **43**(2): 309–320.
8. Gieras JF, Mitchell W. *Permanent Magnet Motor Technology*. Marcel Dekker, Inc.: New York, 2002.
9. Jahns TM. Pulsating torque minimization techniques for permanent-magnet ac motor drives – a review. *IEEE Transactions on Industrial Electronics* 1996; **43**(2): 321–330.
10. Berendsen CS, Champenois G, Bolopion A. Commutation strategies for brushless dc motors: influence on instant torque. *IEEE Transactions on Power Electronics* 1993; **8**(2): 231–236.

11. French P, Acarnley C. Direct torque control of permanent magnet drives. *IEEE Transactions on Industry Applications* 1996; **32**(5): 1080–1088.
12. Park SJ, Park HW, Lee MH, Harashima F. A new approach for minimum-torque-ripple maximum-efficiency control of BLDC motor. *IEEE Transactions on Industrial Electronics* 2000; **47**(1): 109–114.
13. Kang S-J, Sul S-K. Direct Torque Control of Brushless DC Motor with Nonideal Trapezoidal Back EMF. *IEEE Transactions on Power Electronics* 1995; **10**(6): 392–398.
14. Grenier D, Louis JP. Modeling for control of non-sinewave permanent-magnet synchronous drives by extending park's transformation. *Mathematics and Computers in Simulation* 1995; **(38)**(4–6): 445–452.
15. Monteiro JRBA, Oliveira AA Jr. Smooth electromagnetic torque in non-sinusoidal permanent magnet ac machines. *1998 International Conference on Power Electronics Drives and Energy Systems for Industrial Growth*, Vol. 2. Perth: Centre for Renewable Energy Systems and Technologies – CRESTA, 1998; 568–572.
16. Monteiro JRBA, Oliveira AA, Jr., Aguiar ML, Gonzaga DP. Implementation of a non-sinusoidal permanent magnet synchronous machine vectorial control. *IEEE 36th Annual Power Electronics Specialists Conference (PESC05)*, Recife, Brasil, 2005; 2451–2455.
17. Oliveira AA, Jr., Monteiro JRBA, Aguiar ML, Gonzaga DP. Extended dq transformation for vectorial control applications of non-sinusoidal permanent magnet synchronous machines. *IEEE 36th Annual Power Electronics Specialists Conference (PESC05)*, Recife, Brasil, 2005; 1807–1812.
18. Krause PC, Wasynczuk O, Sudhoff SD. *Analysis of Electric Machinery*. IEEE Press: Piscataway, 1996.